Dynamical Signature of Symmetry Fractionalization in Frustrated Magnets

Guang-Yu Sun,[1,2] Yan-Cheng Wang,[3] Chen Fang,[1,4] Yang Qi,[5,6,7] Meng Cheng,[8] and Zi Yang Meng[1,4]

[1]*Beijing National Laboratory of Condensed Matter Physics and Institute of Physics, Chinese Academy of Sciences, Beijing 100190, China*

[2]*School of Physical Sciences, University of Chinese Academy of Sciences, Beijing 100190, China*

[3]*School of Physical Science and Technology, China University of Mining and Technology, Xuzhou 221116, China*

[4]*CAS Center of Excellence in Topological Quantum Computation and School of Physical Sciences, University of Chinese Academy of Sciences, Beijing 100190, China*

[5]*Center for Field Theory and Particle Physics, Department of Physics, Fudan University, Shanghai 200433, China*

[6]*State Key Laboratory of Surface Physics, Fudan University, Shanghai 200433, China*

[7]*Collaborative Innovation Center of Advanced Microstructures, Nanjing 210093, China*

[8]*Department of Physics, Yale University, New Haven, Connecticut 06520-8120, USA*

(Received 5 April 2018; published 14 August 2018)

The nontriviality of quantum spin liquids (QSLs) typically manifests in the nonlocal observables that signify their existence; however, this fact actually casts a shadow on detecting QSLs with experimentally accessible probes. Here, we provide a solution by unbiasedly demonstrating a dynamical signature of anyonic excitations and symmetry fractionalization in QSLs. Employing large-scale quantum Monte Carlo simulation and stochastic analytic continuation, we investigate the extended *XXZ* model on the kagome lattice, and find out that, across the phase transitions from $\mathbb{Z}_2$ QSLs to different symmetry breaking phases, spin spectral functions can reveal the presence and condensation of emergent anyonic spinon and vison excitations, in particular, the translational symmetry fractionalization of the latter, which can be served as the dynamical signature of the seemingly ephemeral QSLs in spectroscopic techniques such as inelastic neutron or resonance (inelastic) x-ray scatterings.

DOI: 10.1103/PhysRevLett.121.077201

Introduction.—Quantum spin liquids (QSLs) [1–4] are exotic phases of matter characterized by long-range many-body entanglement and fractionalized excitations [5]. One of the defining features of QSLs is that there is no local order parameter and the nontriviality of the phase manifests in nonlocal observables. In the case of gapped QSLs, global observables such as Wilson loop operators [6,7], topological entanglement entropies [8–10], and modular transformations [11] have been exploited to characterize topological order theoretically, but none of them are directly accessible in experiments. Available to experiments are measurements of static [12] and dynamical spin correlation functions (besides thermodynamical quantities). In particular, dynamical spin structure factor (DSSF), measured by inelastic neutron scattering, probes the spectral properties of elementary magnetic excitations [13,14]. Therefore, it is an important question for understanding what kind of universal information about the underlying QSLs can be extracted from the momentum and energy resolved DSSFs.

For example, now, a continuum in DSSF is often taken as an indication of fractionalized excitations, but a simple continuum in the spin spectrum can also be caused by disorder [15]. Therefore, additional signatures in DSSF unique to a QSL are desired. On the other hand, it is also desirable to read out more information besides the existence of fractionalized excitations from DSSF. In particular, QSLs with the same type of anyon excitations can be further classified by how internal and lattice symmetries act on the anyons, known as the symmetry-enriched topological order [5,16,17]. It has been proposed that [18–20] this additional information can also be detected from DSSF. In this work, for the first time, we compute the DSSF in a frustrated spin model in an unbiased manner and observe such unique dynamical signatures in DSSF—the fractionalization of lattice symmetries—in QSL with $\mathbb{Z}_2$ topological order.

Model and method.—We consider the extended Balents-Fisher-Girvin (BFG) model on a kagome lattice, where $\mathbb{Z}_2$ QSLs are realized [10,12,21–25]. It has been extensively investigated as one of the very few models of frustrated magnets that can be simulated with unbiased quantum Monte Carlo (QMC) methods, and the defining features of QSL such as spinon and vison excitations [23,26], topological entanglement entropy [10], and fractionalized quantum critical points [24] have been revealed.

The Hamiltonian of the model is given by

$$H = -J_{\pm}\sum_{\langle i,j\rangle}(S_i^+S_j^- + \mathrm{H.c.}) + \frac{J_z}{2}\sum_{\hexagon}\Big(\sum_{i\in\hexagon}S_i^z\Big)^2 + J_z'\sum_{\langle i,j\rangle'}S_i^zS_j^z - h\sum_i S_i^z, \tag{1}$$

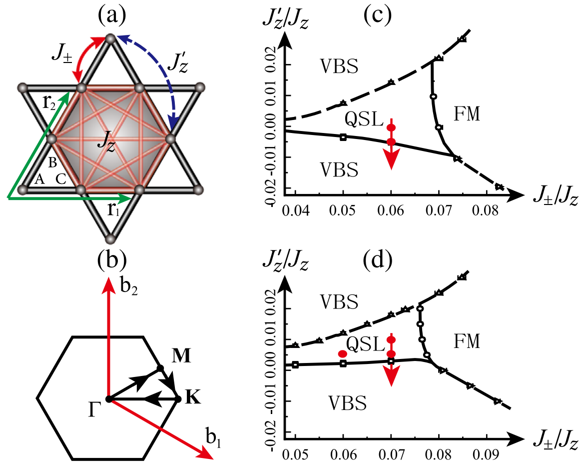

FIG. 1. (a) The kagome lattice with lattice vectors $\mathbf{r}_1$ and $\mathbf{r}_2$, sublattices A, B, and C, and all the interactions $J_\pm$, J_z, and J_z' of the Hamiltonian in Eq. (1) depicted. (b) Brillouin zone of the kagome lattice, with the reciprocal vectors $\mathbf{b}_1$ and $\mathbf{b}_2$, the high symmetry path goes through points Γ, M, and K. (c) $J_\pm/J_z$ vs J_z'/J_z phase diagram of Hamiltonian in Eq. (1) at magnetization $m_z = 0$ [12]. Along the $J_\pm/J_z$ axis, there is a transition from $\mathbb{Z}_2$ QSL to ferromagnetic (FM) ordered phase; along the J_z'/J_z axis, following the direction of the red arrow, there is a transition from $\mathbb{Z}_2$ QSL to a valence bond solid (VBS) phase which orders at point M. (d) $J_\pm/J_z$ vs J_z'/J_z phase diagram of Hamiltonian in Eq. (1) at magnetization $m_z = \frac{1}{6}$ [21]. Along the $J_\pm/J_z$ axis, there is a transition from $\mathbb{Z}_2$ QSL to FM phase; along the J_z'/J_z axis, following the direction of the red arrow, there is a transition from $\mathbb{Z}_2$ QSL to a VBS phase which orders at point Γ.

with the physical meaning of each term illustrated in Fig. 1(a). The original BFG model consists of the nearest-neighbor spin flip $J_\pm > 0$ term, and $J_z > 0$ plaquette interaction term for each hexagon. The newly added J_z' term is a next-nearest-neighbor interaction that frustrates the ordering of spins on the same sublattice [21]. The Zeeman field h tunes the total magnetization. We set $J_z = 1$ as the energy unit. The Hamiltonian preserves all symmetries of the kagome lattice, as well as a $\mathrm{U}(1)_{S_z} \rtimes \mathbb{Z}_2 = \mathrm{O}(2)$ spin symmetry at $h = 0$ and the $\mathrm{U}(1)_{S_z}$ symmetry at $h \neq 0$. Hence, throughout this Letter, the spin quantum number refers to S_z.

To study the model in Eq. (1), we employ large-scale stochastic series expansion [27] QMC simulations. Since the model is highly anisotropic and frustrated, i.e., $J_\pm \ll J_z$ and J_z', to avoid the sampling problem of many local minima, we perform QMC simulations with a five-spin plaquette update (ten legs in a vortex) [12,21]. Moreover, to reduce the rejection rate of the proposed spin configurations, we make use of an algorithm that satisfies the balance condition without imposing detail balance [12,21,28]. The ground state phase diagrams of the model in Eq. (1) at $m_z = 0(\frac{1}{6})$ plateaus are determined in Refs. [12,21,25], and are reproduced in Figs. 1(c) and 1(d). In both cases, stable $\mathbb{Z}_2$ QSL emerges and the transitions from $\mathbb{Z}_2$ QSL to the ferromagnetic (FM) phase driven by $J_\pm/J_z$ are continuous and of $(2+1)$ XY^* universality [21,24].

Spinon and vison continua.—Here, we introduce the concept of spinon and vison excitations in the BFG QSL and develop an understanding of how they are detected in the DSSFs. We are primarily interested in the Ising limit $J_\pm \ll J_z$. Thus, the ground state manifold respects the constraint $S^z = \sum_{i\in\hexagon} S_i^z = 6m_z$ for each hexagon. Violations of these constraints correspond to deconfined excitations, the spinon, whose energy gap is of the order of J_z. Since a spin flip S_i^+, which carries a charge of 1 under $\mathrm{U}(1)_{S_z}$, creates two identical hexagon excitations, each with $S^z = 6m_z + 1$, each of them must carry a $\mathrm{U}(1)_{S_z}$ charge of 1/2 and, thus, is called a spinon. The other kind of excitation, visons, are more subtle and can be viewed as sources of π flux for spinons. When a spinon is transported around a vison, its wave function changes sign. Since visons do not carry any $\mathrm{U}(1)_{S_z}$ charge, it is natural that S^z operators can create pairs of visons. This is supported by an explicit construction of vison states at a soluble deformation of the BFG model in Ref. [22]. Because visons are created in the low-energy manifold with $S^z = 6m_z$, they have a much lower energy gap of the order of $J_\pm^2/J_z$.

Therefore, to observe the spectral information of spinon and vison excitations of $\mathbb{Z}_2$ QSLs, we make use of the following dynamical spin structure factors:

$$S^{\pm}_{\alpha\beta}(\mathbf{q},\tau) = \langle S^+_{-\mathbf{q},\alpha}(\tau) S^-_{\mathbf{q},\beta}(0)\rangle, \tag{2}$$

$$S^{zz}_{\alpha\beta}(\mathbf{q},\tau) = \langle S^z_{-\mathbf{q},\alpha}(\tau) S^z_{\mathbf{q},\beta}(0)\rangle. \tag{3}$$

Here, the imaginary time $\tau \in [0,\beta]$, and to make sure that the system is close to the QSL ground state, we choose $\beta = 2L/J_\pm$ to be below the energy scale associated with the anyonic excitation gap (if $J_\pm = 0.1J_z$, then $T \leq J_\pm^2/J_z$ when $L > 5$). L is the linear system size and the total number of sites $N = 3\times L^2$. α, $\beta = 1, 2, 3$ label the three sublattices of the kagome lattice. $\langle\cdots\rangle$ stands for the QMC ensemble average. We have defined $S^\pm_{\mathbf{q},\alpha} = \sqrt{3/N}\sum_{i\in\alpha} e^{-i\mathbf{q}\cdot\mathbf{r}_i} S_i^\pm$, where the summation over the sublattice α and $\mathbf{r}_i$ is the spatial position of the site i. $S^{zz}_{\mathbf{q},\alpha}$ is defined in the same vein.

One can obtain the real frequency DSSFs via the stochastic analytic continuation (SAC) [29–36] of the imaginary-time data. In SAC, candidate real-frequency spectra are proposed and fitted to the imaginary time data. Each candidate is then weighted by their goodness-of-fit χ^2 as an effective energy, such that a Metropolis sampling can be defined over the proposed spectra. The final spectrum is the ensemble average of all candidates. A detailed account of SAC and its recent applications can be found in Refs. [32–37].

Figure 2 shows the obtained $S^\pm(\mathbf{q},\omega) = \frac{1}{3}\sum_\alpha S^\pm_{\alpha\alpha}(\mathbf{q},\omega)$ and $S^{zz}(\mathbf{q},\omega) = \frac{1}{3}\sum_\alpha S^{zz}_{\alpha\alpha}(\mathbf{q},\omega)$ along the high symmetry

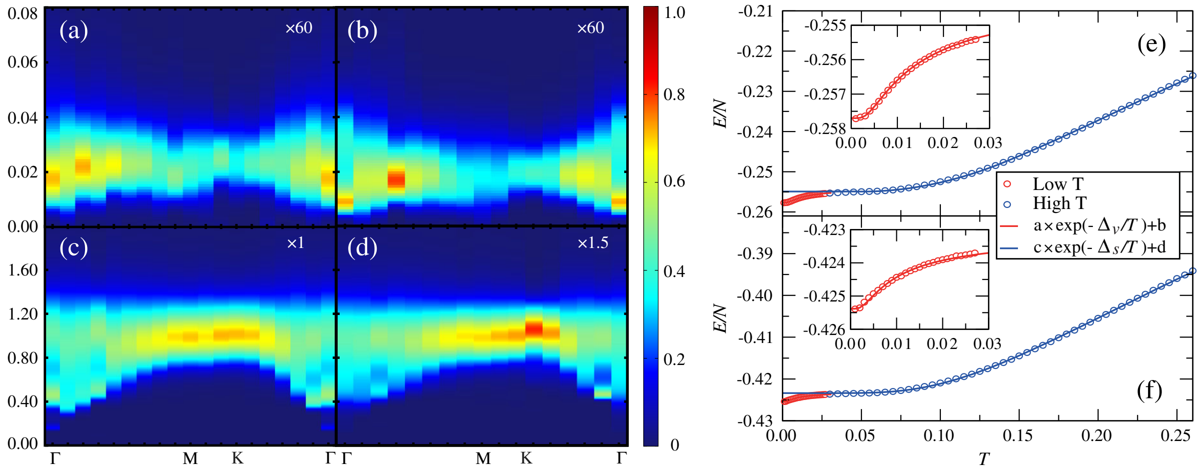

FIG. 2. $S^{zz}(\mathbf{q},\omega)$ along the high symmetry path at $m_z = 0$ with $J_\pm = 0.06$, $J_z' = 0$ (a) and $m_z = \frac{1}{6}$ with $J_\pm = 0.06$, $J_z' = 0.005$ (b). The system size is $L = 16$. The spectra are all gapped with continua. The spectral bottom is at $\omega \sim 0.01$, this is the energy scale of a vison-pair as discussed in the text and consistent with the vison-pair gap (Δ_v) fitted in (e) and (f). $S^{\pm}(\mathbf{q},\omega)$ along the high symmetry path at $m_z = 0$ with $J_\pm = 0.06$, $J_z' = 0$ with $L = 18$ (c) and $m_z = \frac{1}{6}$ with $J_\pm = 0.06$, $J_z' = 0.005$ with $L = 16$ (d). The spectra are all gapped with continua. The spectral bottom is at $\omega \sim 0.2$, consistent with the energy scale of a spinon-pair gap (Δ_s) obtained in (e) and (f). (e) [(f)] is the temperature dependence of the energy for $L = 12$ system for parameters in (a) and (c) [(b) and (d)], $\exp(-\Delta/T)$ fits are performed to extract anyonic gaps.

path. Figures 2(a) and 2(c) are for $m_z = 0$ with $J_\pm = 0.06$, $J_z' = 0$, and Figs. 2(b) and 2(d) are for $m_z = \frac{1}{6}$ with $J_\pm = 0.06$, $J_z' = 0.005$. The parameters are chosen such that the system is well inside the QSL phases, according to the phase diagrams in Figs. 1(c) and 1(d). It is clear that, in both S^x and S^z channels, the spectra are gapped with continua above the gap. As explained earlier, we expect that the magnon spectra observed in $S^\pm$ are comprised of spinon pairs to match the quantum number $S_z = 1$, while the excitations in S^{zz} are comprised of vison pairs to match with $S_z = 0$. Since the spinons and visons are gapped, their pair spectra in $S^\pm(\mathbf{q},\omega)$ and $S^{zz}(\mathbf{q},\omega)$ are gapped as well.

We can confirm this interpretation by examining the energy scales of the spectral gap. We expect that the spinon excitations have a pair gap Δ_s of the order of $J_z = 1$, and for visons, it is $\Delta_v \sim J_\pm^2/J_z$. From Fig. 1, we see that the value of $J_\pm/J_z$ for the onset of the QSL phases is $J_\pm/J_z \sim 0.1$, so we can estimate $\Delta_v \sim 0.01$. In Figs. 2(a)–2(d), we find that the minimum of spectrum is located at the Γ point for both spinons and visons, and we can read off $\Delta_s \approx 0.2$, and $\Delta_v \approx 0.01$, consistent with expectation.

Such consistency in energy scales can also be observed directly from the temperature dependence of the total energy. Figures 2(e) and 2(f) show the $E(T)$ for QSLs at both $m_z = 0$ with $J_\pm = 0.06$, $J_z' = 0$ and $m_z = \frac{1}{6}$ with $J_\pm = 0.06$, $J_z' = 0.005$ for $L = 12$ system. It is clear that there are two different exponential decays in the curves, as shown by our $\exp(-\Delta/T)$ fitting, the higher energy gap is at $\Delta_s \sim 0.42$, which we identify as the spinon-pair gap. It is larger but of the same magnitude with that observed in the $S^\pm(\mathbf{q},\omega)$ in Figs. 2(c) and 2(d), and it is expected, since the thermodynamic measurements contain the contribution from the full spectra, to give rise to a larger gap. The second, much lower $\exp(-\Delta_v/T)$ happens at $\Delta_v \sim 0.01$ (see Fig. 2 insets for clarity), which is apparently the vison-pair gap, consistent with the gap in $S^{zz}(\mathbf{q},\omega)$ in Figs. 2(a) and 2(b). Therefore, we can conclude that the vison-pair excitations are observed in the $S^{zz}(\mathbf{q},\omega)$ spectra and the spinon-pair excitations are observed in the $S^\pm(\mathbf{q},\omega)$ spectra. A similar observation for the vison excitation in the pure BFG model at $m_z = 0$ has also been shown in Ref. [26].

Symmetry fractionalization.—Once we have established the relation between DSSF and anyonic excitation gaps, now, we set out to explore the more salient yet fundamental difference between the $\mathbb{Z}_2$ QSLs at $m_z = 0$ and $\frac{1}{6}$, i.e., their different form of symmetry fractionalization [38–40]. In the case of $\mathbb{Z}_2$ QSLs, spinons and visons can carry a fractional crystal momentum associated with the lattice, which means that

$$T_1^{(a)} T_2^{(a)} = -T_2^{(a)} T_1^{(a)}, \tag{4}$$

here, a refers to an anyon (i.e., spinon or vison) and $T_{1,2}^{(a)}$ denotes the local action of translation on it. Intuitively, with such fractionalization, a moves on a lattice with π flux per unit cell.

The fractional crystal momentum carried by visons is determined by the magnetization per unit cell [41]. In $\mathbb{Z}_2$ QSLs realized in the extended BFG models, the spinon carries a half-integer spin, a fractionalized quantum number [22]. At $m_z = 0$, the spin per unit cell is $\frac{3}{2}$, indicating that there must be an odd number of spinons therein. As a result, moving a vison around a unit cell results in a π Berry phase due to its mutual braiding with the spinons. In other words, the visons must carry a fractional crystal momentum, and consequently, vison translation operators anticommute at $m_z = 0$. On the other hand, at $m_z = \frac{1}{6}$, the spin per unit cell is 1, indicating that there must be an even number of spinons therein. Hence, the visons do not carry a fractional crystal momentum, and the vison translation commutes [42]. There will be two major differences of such fractional crystal momentum in the vison-pair continua at $m_z = 0$ and $\frac{1}{6}$.

First, consider the limit where the spectral edge in DSSF is dominated by scattering states of a pair of visons. If the vison carries a fractional crystal momentum, the density of the scattering states $\mathcal{N}(\mathbf{q}, \omega)$ should exhibit an enhanced periodicity [19,20]

$$\mathcal{N}(\mathbf{q}, \omega) = \mathcal{N}(\mathbf{q} + \mathbf{K}, \omega), \tag{5}$$

where $\mathbf{K}$ is half of the reciprocal vector, i.e., $2\mathbf{K} = \mathbf{G}$. In particular, such enhanced periodicity should manifest in the spectral edge.

Second, the translational symmetry fractionalization is also reflected on the gap-closing momenta near the phase transition driven by vison condensation. Phase transitions between the QSL and nearby symmetry-breaking phases can be understood as driven by anyon condensations: the transition to the FM phase is driven by spinon condensation, and that to the valence bond solid (VBS) phases, both at $m_z = 0$ and $\frac{1}{6}$, are driven by the vison condensation. When the vison carries a fractional crystal momentum, its condensation will lead to the spontaneous breaking of the translational symmetry in the VBS phase. Moreover, the fractional crystal momentum has the following constraints on the ordering wave vector $\mathbf{q}$ of the VBS phase: (i) in the symmetry-breaking phase, the static structure factor must be peaked at $\mathbf{q} + \mathbf{K}$ as well (the peaks do not have the same heights), (ii) if we approach the critical point from the QSL side, we expect to see gap closing in the DSSF at $\mathbf{q}$ and $\mathbf{q} + \mathbf{K}$. Both statements easily follow from the discussion of enhanced periodicity in the density of states of spin excitations if we treat the condensation transition at a "mean-field" level, but they hold more generally even when the interactions between visons can not be ignored.

To detect the translational symmetry fractionalization in the QSLs realized in our model, we monitor how the spectra evolve as the transition to the VBS is approached from the QSL side, indicated by the two paths in Figs. 1(c) and 1(d). These results are shown in Fig. 3. At $m_z = 0$, the envelope of the two-vison continuum shows an enhanced periodicity between $\mathbf{q}$ and $\mathbf{q} + \mathbf{K}$, where the gap closes at both Γ and M. Correspondingly, the static structure factor in the VBS phase is found to have two peaks at Γ and M [see the inset of Fig. 3(a)]. These features are consistent with the expectation that the vison carries a fractional crystal momentum. On the other hand, at $m_z = \frac{1}{6}$, the envelope of the two-vison continuum is asymmetric between Γ and M, the gap closes only at Γ, and the static structure factor in the VBS phase has only one peak at Γ [see the inset of Fig. 3(b)], consistent with the expectation that the vison does not carry a fractional crystal momentum at $m_z = \frac{1}{6}$.

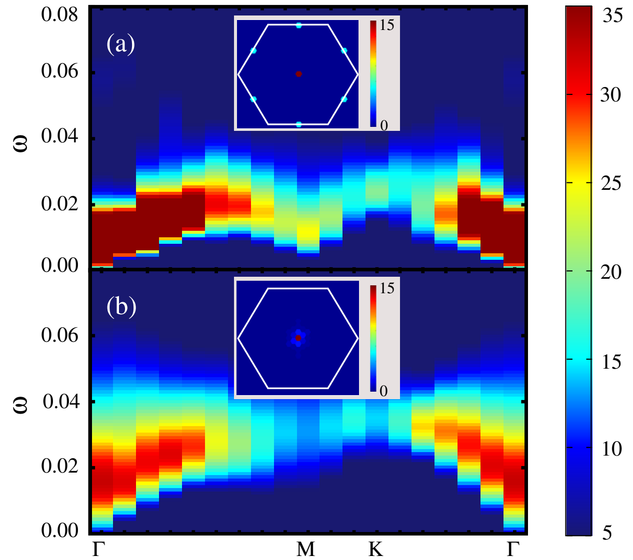

FIG. 3. The comparison of the vison-pair spectra close to the QSL-VBS transition for $m_z = 0$ with $J_\pm = 0.06$, $J'_z = -0.005$ (a) and $m_z = \frac{1}{6}$ with $J_\pm = 0.07$, $J'_z = 0.005$ (b). The system size is $L = 18$. In both cases, $S^{zz}(\mathbf{q}, \omega)$ are becoming gapless due to the vison condensation. However, in (a), the enhanced periodicity manifests in that both points Γ and M become gapless, signifying translational symmetry fractionalization, whereas in (b), there is no enhanced periodicity and, hence, no translational symmetry fractionalization. Insets show the static structure factor of the two VBS phases for $m_z = 0$ and $\frac{1}{6}$, respectively, in (a), the Bragg peaks are at both Γ and M, whereas in (b), only at Γ.

The sharp contrast in Fig. 3 between $m_z = 0$ and $\frac{1}{6}$, both in static and dynamic structure factors, clearly demonstrate the presence or absence of the translation symmetry fractionalization in $\mathbb{Z}_2$ QSLs at the two magnetizations. This is, to our knowledge, for the first time, being observed in a nonperturbative manner. These results point out the possibility that inelastic neutron scattering or resonance (inelastic) x-ray scattering experiments can be further employed to identify gapped QSL on kagome magnets, e.g., in $ZnCu_3(OH)_6Cl_2$ (Herbertsmithite) [13,43] and $Cu_3Zn(OH)_6FBr$ (Zn-doped Barlowite) [14,44–49]. In both cases, existing experimental data are pointing towards gapped QSL ground states with possibly $\mathbb{Z}_2$ topological order, especially the latter, in which a gapped spinon continuum has been consistently revealed from both NMR [44] and inelastic neutron scattering experiments [14]. If, when driving the material through a transition from QSL to ordered state, the doubled period could be observed in DSSF, such a dynamical signature of symmetry fractionalization will be the decisive information to confirm the $\mathbb{Z}_2$ QSL in materials.

Discussion.—Employing large-scale QMC + SAC simulations, we study the DSSF in extended BFG models at different magnetizations. We associate the DSSF of S^zS^z and S^+S^- operators with the two-particle continua of the vison and spinons. The two-vison continuum reveals the difference in translation-symmetry fractionalization between QSLs at different m_z: at $m_z = 0$, the continuum has an enhanced periodicity relating Γ and M points, meaning that the vison carries the symmetry fractionalization. In contrast, at $m_z = \frac{1}{6}$, the continuum has no such enhanced periodicity, meaning that the vison carries a trivial symmetry fractionalization, instead. Furthermore, at $m_z = 0$, this enhanced periodicity also implies that the condensation of visons must occur simultaneously at Γ and M and, thus, breaks translation symmetries. Correspondingly, the condensation of visons at $m_z = \frac{1}{6}$ leads to a translational symmetric VBS state [21]. Therefore, the dispersion of the two-vison continuum observed in the DSSF, together with the nature of the vison-condensation transition, reveals the symmetry fractionalization pattern of the anyonic excitations in QSL.

Our findings show that the DSSF can not only detect the existence of fractionalized anyonic excitations in a QSL, but also distinguish different symmetry-fractionalization patterns carried by the anyons. Since DSSF can be measured in different experimental probes, our findings not only have theoretical importance in understanding the properties of the topological state of matter, but also provide a valuable experimental guide to look for the dynamical signature of symmetry-enriched topological order in QSL materials.

We would like to thank Stefan Wessel for communicating results of a related investigation [50] prior to publication and Anders Sandvik for valuable discussions. G. Y. S., Y. C. W., and Z. Y. M. acknowledge funding from the Ministry of Science and Technology of China through the National Key Research and Development Program under Grant No. 2016YFA0300502, from the key research program of the Chinese Academy of Sciences under Grant No. XDPB0803 and from the National Science Foundation of China under Grants No. 11421092, No. 11574359, and No. 11674370 as well as the National Thousand-Young Talents Program of China. Y. Q. is supported by the Ministry of Science and Technology of China under Grant No. 2015CB921700. M. C. is supported by startup funds from Yale University. We thank the Center for Quantum Simulation Sciences in the Institute of Physics, Chinese Academy of Sciences, the Tianhe-1A platform at the National Supercomputer Center in Tianjin for their technical support and generous allocation of CPU time.

[1] L. Balents, Nature (London) **464**, 199 (2010).
[2] Y. Zhou, K. Kanoda, and T.-K. Ng, Rev. Mod. Phys. **89**, 025003 (2017).
[3] L. Savary and L. Balents, Rep. Prog. Phys. **80**, 016502 (2017).
[4] Y. Zhou, K. Kanoda, and T.-K. Ng, Rev. Mod. Phys. **89**, 025003 (2017).
[5] X.-G. Wen, Rev. Mod. Phys. **89**, 041004 (2017).
[6] K. Gregor, D. A. Huse, R. Moessner, and S. L. Sondhi, New J. Phys. **13**, 025009 (2011).
[7] D. N. Sheng and L. Balents, Phys. Rev. Lett. **94**, 146805 (2005).
[8] A. Kitaev and J. Preskill, Phys. Rev. Lett. **96**, 110404 (2006).
[9] M. Levin and X.-G. Wen, Phys. Rev. Lett. **96**, 110405 (2006).
[10] S. V. Isakov, M. B. Hastings, and R. G. Melko, Nat. Phys. **7**, 772 (2011).
[11] Y. Zhang, T. Grover, A. Turner, M. Oshikawa, and A. Vishwanath, Phys. Rev. B **85**, 235151 (2012).
[12] Y.-C. Wang, C. Fang, M. Cheng, Y. Qi, and Z. Y. Meng, arXiv:1701.01552.
[13] T.-H. Han, J. S. Helton, S. Chu, D. G. Nocera, J. A. Rodriguez-Rivera, C. Broholm, and Y. S. Lee, Nature (London) **492**, 406 (2012).
[14] Y. Wei, Z. Feng, W. Lohstroh, C. dela Cruz, W. Yi, Z. F. Ding, J. Zhang, C. Tan, L. Shu, Y.-C. Wang, J. Luo, J.-W. Mei, Z. Y. Meng, Y. Shi, and S. Li, arXiv:1710.02991.
[15] Z. Ma, J. Wang, Z.-Y. Dong, J. Zhang, S. Li, S.-H. Zheng, Y. Yu, W. Wang, L. Che, K. Ran, S. Bao, Z. Cai, P. Cermák, A. Schneidewind, S. Yano, J. S. Gardner, X. Lu, S.-L. Yu, J.-M. Liu, S. Li *et al.*, Phys. Rev. Lett. **120**, 087201 (2018).
[16] M. Barkeshli, P. Bonderson, M. Cheng, and Z. Wang, arXiv:1410.4540.
[17] N. Tarantino, N. H. Lindner, and L. Fidkowski, New J. Phys. **18**, 035006 (2016).
[18] X.-G. Wen, Phys. Rev. B **65**, 165113 (2002).
[19] A. M. Essin and M. Hermele, Phys. Rev. B **90**, 121102 (2014).
[20] J.-W. Mei and X.-G. Wen, arXiv:1507.03007.
[21] Y.-C. Wang, X.-F. Zhang, F. Pollmann, M. Cheng, and Z. Y. Meng, arXiv:1711.03679 [Phys. Rev. Lett. (to be published)].
[22] L. Balents, M. P. A. Fisher, and S. M. Girvin, Phys. Rev. B **65**, 224412 (2002).
[23] S. V. Isakov, Y. B. Kim, and A. Paramekanti, Phys. Rev. Lett. **97**, 207204 (2006).
[24] S. V. Isakov, R. G. Melko, and M. B. Hastings, Science **335**, 193 (2012).
[25] Y.-C. Wang, G.-Y. Sun, X.-F. Zhang, and Z. Y. Meng (to be published).
[26] S. V. Isakov, A. Paramekanti, and Y. B. Kim, Phys. Rev. B **76**, 224431 (2007).
[27] O. F. Syljuåsen and A. W. Sandvik, Phys. Rev. E **66**, 046701 (2002).
[28] H. Suwa and S. Todo, Phys. Rev. Lett. **105**, 120603 (2010).
[29] A. W. Sandvik, Phys. Rev. B **57**, 10287 (1998).
[30] K. S. D. Beach, arXiv:cond-mat/0403055.
[31] O. F. Syljuåsen, Phys. Rev. B **78**, 174429 (2008).
[32] A. W. Sandvik, Phys. Rev. E **94**, 063308 (2016).
[33] Y. Q. Qin, B. Normand, A. W. Sandvik, and Z. Y. Meng, Phys. Rev. Lett. **118**, 147207 (2017).
[34] H. Shao and A. W. Sandvik (to be published).
[35] H. Shao, Y. Q. Qin, S. Capponi, S. Chesi, Z. Y. Meng, and A. W. Sandvik, Phys. Rev. X **7**, 041072 (2017).
[36] C.-J. Huang, Y. Deng, Y. Wan, and Z. Y. Meng, Phys. Rev. Lett. **120**, 167202 (2018).
[37] Y.-R. Shu, M. Dupont, D.-X. Yao, S. Capponi, and A. W. Sandvik, Phys. Rev. B **97**, 104424 (2018).

[38] Y. Qi and L. Fu, Phys. Rev. Lett. **115**, 236801 (2015).
[39] Y. Qi and L. Fu, Phys. Rev. B **91**, 100401(R) (2015).
[40] Y. Qi, M. Cheng, and C. Fang, arXiv:1509.02927.
[41] M. Cheng, M. Zaletel, M. Barkeshli, A. Vishwanath, and P. Bonderson, Phys. Rev. X **6**, 041068 (2016).
[42] See Supplemental Material at http://link.aps.org/supplemental/10.1103/PhysRevLett.121.077201 for details of the vison translational symmetry fractionalization, the consequential enhanced periodicity of density of states in DSSF, and the finite size effects in the obtained $S^{zz}(\mathbf{q},\omega)$ from the QMC + SAC simulations.
[43] M. Fu, T. Imai, T.-H. Han, and Y. S. Lee, Science **350**, 655 (2015).
[44] Z. Feng, Z. Li, X. Meng, W. Yi, Y. Wei, J. Zhang, Y.-C. Wang, W. Jiang, Z. Liu, S. Li, F. Liu, J. Luo, S. Li, G.-q. Zheng, Z. Y. Meng, J.-W. Mei, and Y. Shi, Chin. Phys. Lett. **34**, 077502 (2017).
[45] X.-G. Wen, Chin. Phys. Lett. **34**, 090101 (2017).
[46] Z. Feng, Y. Wei, R. Liu, D. Yan, Y.-C. Wang, J. Luo, A. Senyshyn, C. dela Cruz, W. Yi, J.-W. Mei, Z. Y. Meng, Y. Shi, and S. Li, arXiv:1712.06732.
[47] C. M. Pasco, B. A. Trump, T. T. Tran, Z. A. Kelly, C. Hoffmann, I. Heinmaa, R. Stern, and T. M. McQueen, Phys. Rev. Mater. **2**, 044406 (2018).
[48] K. M. Ranjith, C. Klein, A. A. Tsirlin, H. Rosner, C. Krellner, and M. Baenitz, Sci. Rep. **8**, 10851 (2018).
[49] Z. Feng, W. Yi, K. Zhu, J. Ma, J. Luo, S. Li, Z. Y. Meng, and Y. Shi, arXiv:1806.00803.
[50] J. Becker and S. Wessel, following Letter, Phys. Rev. Lett. **121**, 077202 (2018).